Carbohydrate Polymers 93 (2013) 518–527

Contents lists available at SciVerse ScienceDirect

Carbohydrate Polymers

journal homepage: www.elsevier.com/locate/carbpol

Selective adsorption of hemoglobin using polymer-grafted-magnetite nanocellulose composite

Thayyath Sreenivasan Anirudhan*, Sylaja Raveendran Rejeena

Department of Chemistry, University of Kerala, Kariavattom, Trivandrum-695 581, India

ARTICLE INFO

Article history:
Received 17 January 2012
Received in revised form
24 November 2012
Accepted 26 November 2012
Available online 4 January 2013

Keywords:
Graft copolymerization
Nanocellulose
Adsorption
Hemoglobin
Isotherm
Desorption

ABSTRACT

A novel adsorbent, poly(methacrylic acid-co-vinyl sulfonic acid)-grafted-magnetite nanocellulose composite (P(MAA-co-VSA)-g-MNCC) was synthesized for adsorbing hemoglobin (Hb) selectively from aqueous solutions. FTIR, XRD and DLS analyses were carried out to characterize the material. Hb exhibited a decrease in α-helix and an increase in β-sheet structure, upon immobilization onto P(MAA-co-VSA)-g-MNCC. The maximum adsorption was found to be at pH 6.5 with a monolayer capacity of 248.19 mg/g at 30 °C. Adsorption capacity attained saturation within 2 h. The kinetic data were found to follow pseudo-second-order model which is based on chemisorption. Adsorption behavior was observed to be endothermic in nature. P(MAA-co-VSA)-g-MNCC can be used in the selective adsorption of Hb from mixture of proteins. Spent adsorbent was effectively regenerated with 0.01 M KOH. Present investigation had shown that P(MAA-co-VSA)-g-MNCC would be a promising material for the selective recovery of Hb from aqueous solutions.

1. Introduction

The selective separation of biomolecules such as proteins from mixtures is a challenging problem faced in biotechnological and biomedical fields. To date, various methods have been developed for the separation of proteins, including ultra filtration, electrophoretic separation, liquid chromatography, adsorption, and membrane chromatography (El-Safty, Shahat, & Nguyen, 2011). Among these, adsorption is considered to be an effective technique in the selective separation of proteins (Anirudhan & Senan, 2011; Shukoor et al., 2007). The greatest incentive for research in the domain of protein adsorption on solid surfaces arises from the numerous technological and medical applications that depend on this phenomenon (Bajpal & Sachdeva, 2002). Low cost adsorbents with high adsorption capacities are still under development to reduce the adsorbent dose and minimize the disposal problems. Many workers reported that cellulose is a good adsorbent for recovering proteins from aqueous solutions (Anirudhan, Tharun, & Rejeena, 2011), because of its abundant resources, low production cost and biodegradability. Cellulose-based superabsorbents gained much attention for a specified application, such as agriculture, hygienic products, separation processes, wastewater treatment and drug release. However poor mechanical strength, low sorption capacity and microbial contamination limit the application of cellulose as a potential adsorbent. The individualization of cellulose nanofibre from renewable sources is found to be a solution in recent years because of their exceptional mechanical properties (high specific strength and modulus), large specific surface area, and low coefficient of thermal expansion, high aspect ratio and environmental benefits (Nishino, Matsuda, & Hirao, 2004). Graft copolymerization can be used for further improving mechanical strength, thermal stability and hydrophilicity, and tailoring of desired functionalities in the polymer which will help in the targeted extraction of proteins from mixtures.

The encapsulation of magnetic nanomaterials like Fe_3O_4 in the polysaccharide matrix will increase the biocompatibility, colloidal stability, the surface to volume ratio and makes the particles for use in adsorptive separation (Dias, Hussain, Marcos, & Roque, 2011). Nanosized magnetite (Fe_3O_4) particles are the most commonly used carriers for the extraction of biologically active compounds owing to their higher saturation magnetism, low toxicity, larger specific surface area and easy manipulation of surface modification (Peng, Hidajat, & Uddin, 2004). The magnetic properties of the Fe_3O_4 will enable to achieve the rapid separation of the adsorbent in magnetic field, via magnetic fishing (Bayramoglu, Yilmaz, Senel, & Arica, 2008).

In the present study, we synthesized a novel multi-component superabsorbent composite by graft copolymerization of vinyl monomers onto magnetite nanocellulose composite. Methacrylic acid (MAA) and vinyl sulfonic acid (VSA) were chosen as vinyl monomers because of its anionic character, which increase the swelling capacity of the material (Bao, Ma, & Li, 2011). Hemoglobin

* Corresponding author. Tel.: +91 471 2416472; fax: +91 0471 2307158.
E-mail address: tsani@rediffmail.com (T.S. Anirudhan).

0144-8617/$ – see front matter © 2012 Elsevier Ltd. All rights reserved.
http://dx.doi.org/10.1016/j.carbpol.2012.11.104

(Hb) was chosen as a model protein to study the adsorption behavior on the newly developed adsorbent, poly(methacrylic acid-co-vinyl sulfonic acid)-grafted magnetite nanocellulose composite (P(MAA-co-VSA)-g-MNCC). Hb is a globular protein that carries oxygen (O_2) molecules and carbon dioxide (CO_2) molecules throughout the body. It is found in red blood cells, in mammals and other animals, and can be used as artificial blood substitutes. Batch adsorption experiments were conducted to evaluate the Hb adsorption behavior onto P(MAA-co-VSA)-g-MNCC. Selectivity of the adsorbent in the recovery of Hb was tested by conducting adsorption experiments with mixture of proteins.

2. Materials and methods

2.1. Materials

Saw dust of *Mangiferra indica* (collected from Local saw mill, Trivandrum) was used after thorough washing and drying at 80 °C. Hb (pI = 6.8), with a MW of 68 kDa was obtained from Sino-America Biotechnology Company. BSA (pI = 4.9), with a MW of 67 kDa was of monomer grade from Sigma (Milwaukee, WI, USA). MAA, VSA and ethyleneglycoldimethacrylate (EGDMA) were obtained from Sigma–Aldrich, Milwau-kee, WI, USA. Potassium persulfate ($K_2S_2O_8$), sulfuric acid, ammonia solution, hydrochloric acid, sodium chloride, urea and sodium hydroxide were procured from E-Merck (Worli, Mumbai, India). Ferric chloride hexahydrate ($FeCl_3{\cdot}6H_2O$) (98%), ferrous sulfate heptahydrate ($FeSO_4{\cdot}7H_2O$) (99%) were obtained from Fisher, USA. All the reagents were of analytical grade and used without further purification. All stock solutions were prepared in double distilled water.

2.2. Preparation of P(MAA-co-VSA)-g-MNCC

The general procedure adopted for the preparation of P(MAA-co-VSA)-g-MNCC consists of four steps.

Step 1. Extraction of cellulose from saw dust

Saw dust was pretreated with 10% H_2SO_4 solution (120 °C, 10 min) and centrifuged to remove the pentosan rich solution. Delignification was achieved by the subsequent treatment with 1% NaOH (100 °C, 1 h). The obtained brown mass was bleached with 5% H_2O_2 (80 °C, 1 h) yielded white cellulose as the product (Mulinari & Da Silva, 2008).

Step 2. Preparation of nanocellulose (NC) from cellulose

About 5 g of cellulose was combined with 250 mL distilled water under magnetic stirring (20 min). Sulfuric acid (98%, 140 mL) was dropped to the cooled cellulose suspension (250 mL, 20 °C). After complete addition, the suspension was heated at 50 °C for 2 h. The hot mixture was diluted ten times with ice cooled distilled water. The obtained white colloid was centrifuged, washed many times with water and freeze-dried (Capadona et al., 2009).

Step 3. Preparation of magnetite nanocellulose composite (MNCC)

Magnetite nanocellulose composite was prepared by co-precipitating Fe(II) and Fe(III) ions in aqueous solution containing NC with ammonia. Briefly, about 1.5 g of NC was added to 200 mL distilled water and stirred for 10 min. To the mixture, 1.49 g $FeCl_3{\cdot}6H_2O$ and 0.765 g $FeSO_4{\cdot}7H_2O$ were added to form a source of iron, and heated at 60 °C. Chemical precipitation was achieved by adding 8.0 M ammonia solution dropwise with vigorous stirring and a constant pH of 10, upon which an orange color suspension obtained was changed to a black precipitate. After incubation for 4 h at 60 °C the mixture was cooled to room temperature with stirring, and the resulting MNCC particles were separated magnetically. The product thus obtained was washed several times with distilled water, finally with ethanol and dried.

Step 4. Preparation of P(MAA-co-VSA)-g-MNCC

The general procedure adopted for the preparation of P(MAA-co-VSA)-g-MNCC is illustrated in Scheme 1. Typically, about 0.5 g of MNCC was stirred well with 100 mL distilled water (60 °C, 20 min). $K_2S_2O_8$ (0.004 M, 0.92 g) was added and kept at 60 °C for 10 min. After cooling the suspension to 40 °C, a mixture of MAA (0.1 M, 8.5 mL), VSA (0.1 M, 7.8 mL) and EGDMA (0.015 M, 2.83 mL) were added. The pH was adjusted by NaOH to 10. The temperature was risen to 70 °C and maintained for 2 h to complete the reaction. The obtained product was filtered and washed repeatedly with distilled water and ethanol to remove excess chemicals and then dried in vacuum at 70 °C. The dried sample was then grounded and sieved to obtain −80 +230 mesh size particles (average diameter of 0.096 mm).

2.3. Instruments and method of characterization

The Fourier transform infrared (FTIR) spectra were recorded with a Shimadzu FTIR spectrometer in the wavelength range 400–4000 cm^{-1} using a KBr window at a resolution of 4 cm^{-1}. Powder X-ray diffraction patterns (XRD) of the samples were taken in an X'Pert Pro X-ray diffractometer using nickel filtered CuKα radiation at a scanning speed of 2°/min and at a wavelength of 1.5406 Å. Dynamic Light Scattering measurements for the NC were carried out in a laser scattering particle size distribution analyzer from Malvern Instruments Ltd. Water was used as the dispersant with refractive index 1.33 and viscosity 0.8872 cP. The concentration of protein solution was determined spectrophotometrically on a JASCO UV–visible (model V-530, India) spectrophotometer. The specific surface area was measured by BET N_2 adsorption using a Quantasorb surface analyzer (model QS/7, USA). The pH measurements were made using a systronic microprocessor pH meter (model μ-362, India). A potentiometric titration method (Schwarz, Driscoll, & Bhanot, 1984) was used to determine the pH of point of zero charge (pHpzc). A temperature controlled water bath shaker (Labline, India) with a temperature tolerance of ±1 °C was used for sorption studies.

2.4. Determination of sulfonyl and carboxyl groups

The total amount of acidic functional groups present in the adsorbent was determined as follows. To about 50 mg of the adsorbent, 20 mL 0.01 M NaCl solution was added and shaken for 1 h. The solution was filtered and filtrate was titrated against 0.01 M NaOH using phenolphthalein as indicator. Boehm titration was performed to determine the amount of free carboxyl (–COOH) groups. About 0.15 g of powdered adsorbent was shaken with 30 mL $NaHCO_3$ for 20 h, and filtered. An aliquot of the filtrate was mixed with excess of 0.05 M HCl and the CO_2 gas formed was boiled off and back titrated with 0.05 M NaOH. Subtraction of the amount of carboxyl group content from the total acidic group content provided the amount of sulfonyl ($-SO_3H$) groups present in P(MAA-co-VSA)-g-MNCC.

2.5. Swelling measurements

A known quantity of P(MAA-co-VSA)-g-MNCC (0.1 g) was taken in a weighed tea bag and immersed in 50 mL aqueous solutions of desired pH (2.0–9.0) and allow to soak at constant temperature of 30 °C. After a suitable period, the equilibrated swollen adsorbent was allowed to drain by removing the tea bag from water and hanging until no drop drained. The bag was then weighed to determine the weight of the swollen adsorbent. The swelling capacity was

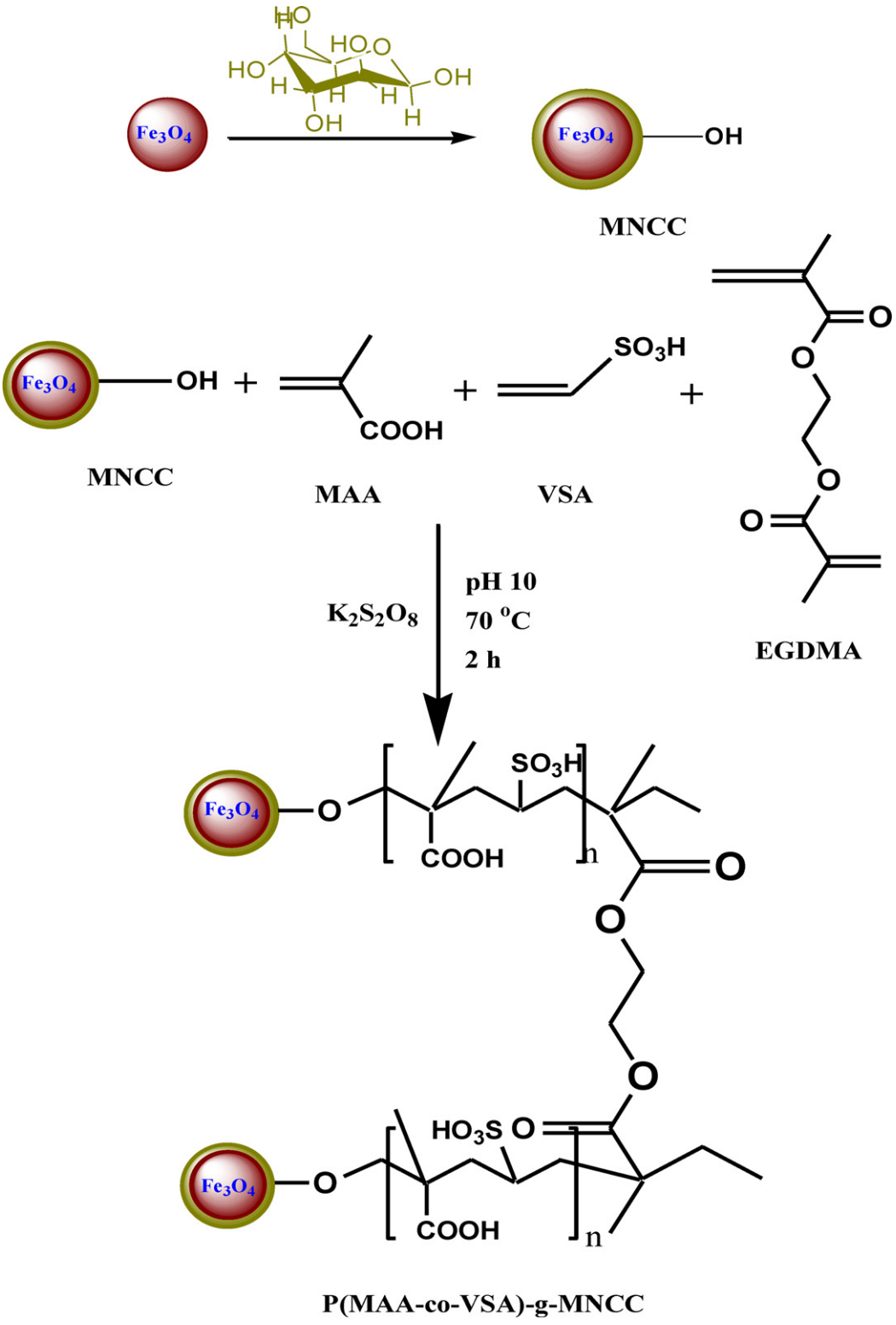

Scheme 1. Proposed reaction mechanism for the synthesis of P(MAA-co-VSA)-g-MNCC.

calculated using the following equation (Pal, Banthia, & Majumdar, 2009).

$$\text{Swelling}(\%) = \frac{W_s - W_d}{W_d} \times 100 \quad (1)$$

where W_s is the weight of the swollen sample and W_d is the weight of the dry sample. The swelling experiments were also carried out with different temperatures (10–40 °C) at neutral pH, and predetermined time intervals.

2.6. Adsorption experiments

Batch experiments were carried out by shaking 0.1 g P(MAA-co-VSA)-g-MNCC with 50 mL aqueous solutions of Hb of the desired

initial concentration (25–800 mg/L) and pH (adjusted using HCl or NaOH) in different glass-stoppered Erlenmeyer flasks at 200 rpm for predetermined time intervals (5–240 min) and temperatures (10–40 °C). Then, the suspension was centrifuged at regular intervals to separate the adsorbents from the solution and the Hb concentration in the supernatant solution was measured in UV–vis spectrophotometer at 406 nm (Fargues, Bailly, & Grevillot, 1998). The adsorbed amounts of Hb on the adsorbent q_e (mg/g) were calculated from the mass balance equation as:

$$q_e = (C_0 - C_e) \times \frac{V}{m} \quad (2)$$

$$Adsorption(\%) = \frac{(C_0 - C_e)}{C_0} \times 100 \quad (3)$$

where C_0 and C_e (mg/L) are the initial Hb concentration and the Hb concentration in the solution at adsorption equilibrium respectively, V (mL) is the volume of the Hb solution and m (g) is the adsorbent mass. The measurements were made for each sample and the results were averaged. The maximum variation with batch adsorption data among triplicate values was 4.4%.

2.7. Desorption and regeneration experiments

Desorption experiments were conducted by shaking 0.1 g of Hb-loaded P(MAA-co-VSA)-g-MNCC (Hb-P(MAA-co-VSA)-g-MNCC) with 50 mL of 0.01 M CH_3COOH, KOH, $H_2C_2O_4$, Na_2CO_3 and Na_2SO_4 solutions for a period of 2 h at 30 °C. After centrifugation, the concentrations of Hb in the solutions were determined spectrophotometrically. The desorption percentage of Hb from P(MAA-co-VSA)-g-MNCC was calculated from the adsorption and desorption data using the following equation:

$$\text{Hb desorbed}(\%) = \frac{M_d}{M_a} \times 100 \quad (4)$$

where M_d (mg/g) is the amount of Hb desorbed by reagents, M_a (mg/g) is the amount of Hb adsorbed onto P(MAA-co-VSA)-g-MNCC. Regeneration studies were carried out using 0.01 M KOH as the desorbing agent for five adsorption–desorption cycles.

3. Results and discussion

3.1. Synthesis and properties of the adsorbent

Adsorbent preparation procedure is represented in Scheme 1. P(MAA-co-VSA)-g-MNCC was synthesized by graft copolymerization of MAA and VSA onto MNCC, in the presence of EGDMA as cross linking agent and $K_2S_2O_8$ as free radical initiator. Initially, the persulfate initiator ($K_2S_2O_8$) generates anionic radical KSO_4^-. This anionic radical abstracts hydrogen from the hydroxyl group of the MNCC to form macroradicals (MNCC–O•). The macroradical is added to the double bond of the monomer resulting in a covalent bond between the monomer and the MNCC and a chain gets initiated. Both the monomers form radicals, so the hydrophilicity determines the group which added first. Previous reports mention that the hydrophilic chain enhances the addition of a hydrophilic monomer (Kundakci, Uzum, & Karadag, 2008). MNCC has hydrophilic hydroxyl groups and therefore, the MAA group (hydrophilic monomer) gets attached first followed by VSA (hydrophobic monomer). Since a crosslinking agent (EGDMA) is in the system, an interpenetrating polymer is formed with $-SO_3H$ and –COOH functionalities at chain end.

The amount of sulfonyl and carboxyl functional groups in P(MAA-co-VSA)-g-MNCC was estimated to be 1.92 and 1.36 meq/g, respectively, was an evidence for proper grafting of PMAA and PVSA onto MNCC. The specific surface area of Cellulose and P(MAA-co-VSA)-g-MNCC was found to be 22.7 and 112.36 m^2/g, respectively.

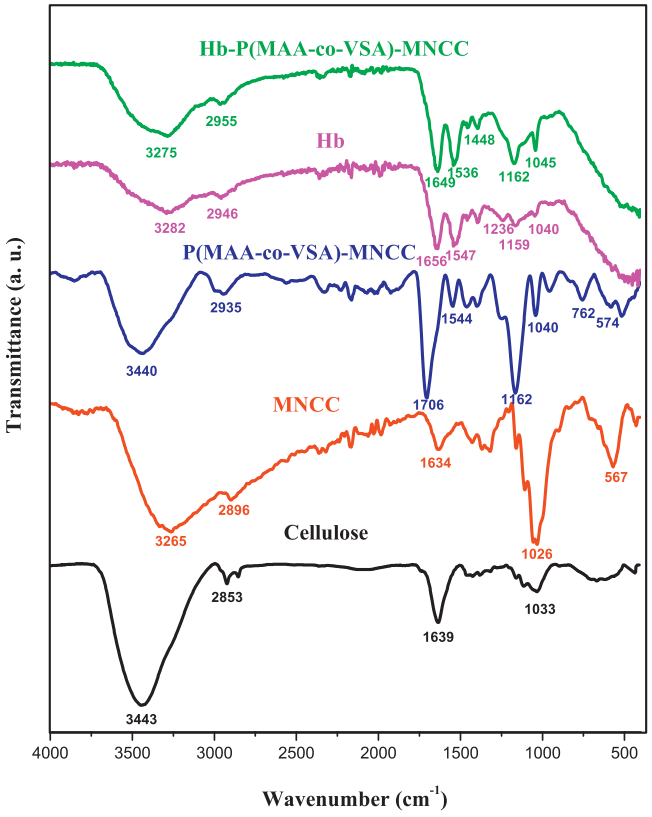

Fig. 1. FTIR spectra of cellulose, MNCC, P(MAA-co-VSA)-g-MNCC, Hb and Hb-P(MAA-co-VSA)-g-MNCC.

The zero point charge (pH_{zpc}) of Cellulose and P(MAA-co-VSA)-g-MNCC was observed at pH 5.5 and 3.6, respectively. The decreased pH_{zpc} of the adsorbent may be due to the presence of large amount of easily ionizable $-SO_3H$ and –COOH groups anchored on the surface.

3.2. Characterization studies

The FTIR spectra of Cellulose, MNCC, P(MAA-co-VSA)-g-MNCC, Hb and Hb- P(MAA-co-VSA)-g-MNCC (Fig. 1) show absorption bands at 3344, 2900 and 1640 cm^{-1} due to hydrogen bonded O—H stretching vibration, C—H stretching from the $-CH_2$ group and –OH bending vibration, respectively. The bands at 1426, 1382 and 1315 cm^{-1} are due to the bending vibration of C—H stretching from the $-CH_2$ group. The bands at 1160 and 1078 cm^{-1} are due to antisymmetric stretching vibrations of the C—O—C bridge and skeletal vibrations involving C—O stretching, respectively; which are assigned to the characteristics of the saccharide structure. Appearance of an absorption band at 897 cm^{-1} is attributed to the glucosidic ring in cellulose structure. In FTIR spectra of MNCC, there was a high intensity broad band at around 566 cm^{-1}, which is the characteristic absorption band of Fe—O in the tetrahedral sites (Nyquist & Kagel, 1971). The small shift in the stretching peaks of O—H (3260 cm^{-1}) in the presence of Fe_3O_4 indicating that an interaction exists between the Cellulose and magnetic core. The characteristic absorption bands of Cellulose retained in MNCC with a small decrease in intensity indicates the degradation of the hydrogen bond between the cellulosic chains during the acid hydrolysis treatment (Abdel, Zeinab, El-Wahab, Ibrahim, & Al-Shemy, 2010). The characteristic absorption bands of $-SO_3H$ group at 1163, 1039 and 590 cm^{-1} (Anirudhan & Senan, 2011), and sharp adsorption peak at 1712 cm^{-1} (ester carbonyl group) confirms the graft copolymerization of MNCC with VSA and MAA. Hb shows peaks

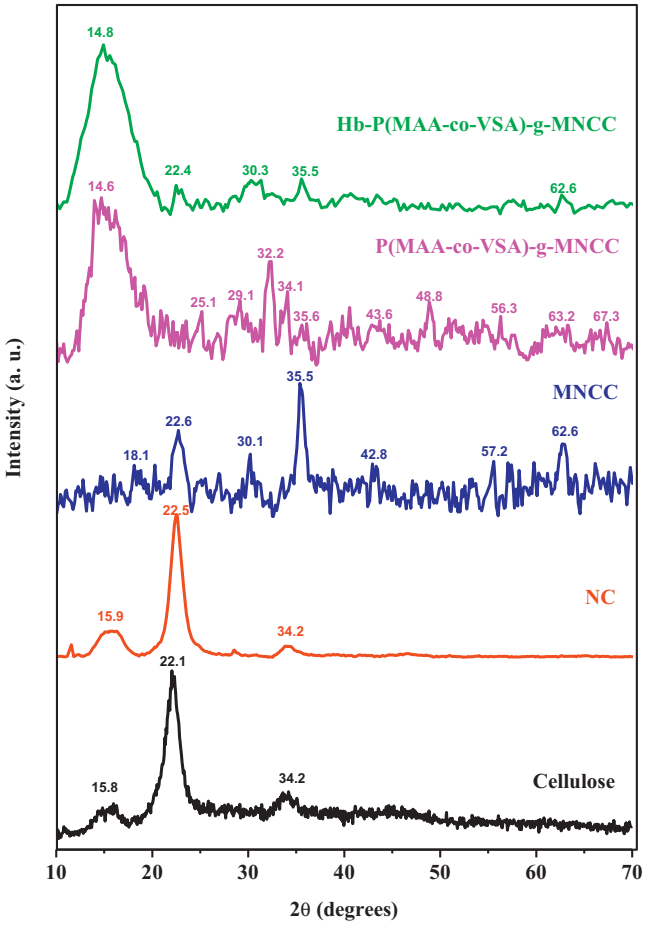

Fig. 2. XRD patterns of cellulose, NC, MNCC, P(MAA-co-VSA)-g-MNCC and Hb-P(MAA-co-VSA)-g-FMNC.

at 3270 cm^{-1} (stretching vibration of primary amine), 1391 cm^{-1} (C—N stretching vibration of aromatic amine), 1532 cm^{-1} (amide-II) and 1639 cm^{-1} (amide-I). In the FTIR spectrum of Hb-P(MAA-co-VSA)-MNCC, the characteristic peak correspond to α-helix conformation (1633 cm^{-1}) and amide II frequency (1540 cm^{-1}) are present which suggests the adsorption of Hb on the surface of P(MAA-co-VSA)-g-MNCC (Haynes and Norde, 1994; Joon and Kim, 2000).

To determine the conformational stability of Hb in adsorbed state, secondary structure was evaluated by fitting the Gaussian curve on the amide I band of the FTIR spectra of Hb and Hb-P(MAA-co-VSA)-g-MNCC (Fig. S1) and the results obtained are listed in Table S1 (Cruz, Pfromm, Tomich, & Rezac, 2010). Hb exhibits a decrease in α-helix, random coil and turn contents and an increase in β-sheet and intermolecular β aggregates, upon immobilization onto P(MAA-co-VSA)-g-MNCC. A decrease in α-helix and increase in β-structure can be observed when proteins are adsorbed onto a polymer surface (Ishiguro et al., 2005; Yokoyama et al., 2003). The increase in β-sheet structure clearly shows the increased conformational stability of Hb onto P(MAA-co-VSA)-g-MNCC.

Supplementary data related to this article found, in the online version, at http://dx.doi.org/10.1016/j.carbpol.2012.11.104.

The XRD patterns of Cellulose, NC, MNCC, P(MAA-co-VSA)-g-MNCC, Hb-P(MAA-co-VSA)-g-MNCC are shown in Fig. 2. The XRD pattern of Cellulose shows peaks at 2θ values of 22.1° and 34.2° correspond to crystalline domain of cellulose structure where as the broad hump at 15.8° indicates the amorphous nature of cellulose. Eventhough, the characteristic peaks of NC are same as that of Cellulose, its broadness increased to

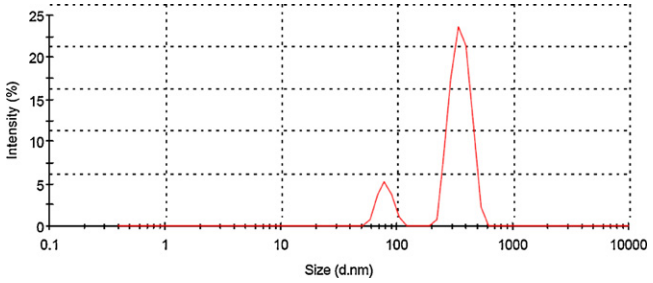

Fig. 3. Particle size distribution of NC.

a small extent, which may be due to the small particle size and strain induced during the conversion to nanoregime. The sharper diffraction peaks of NC were aroused due to the partial removal of the amorphous regions during the acid hydrolysis treatment of cellulose (Alemdar & Sain, 2008). The distinct peaks occur at 2θ of 18.1°, 30.1°, 35.5°, 42.8°, 57.2° and 62.6° in MNCC reveals the presence of pure Fe_3O_4 with spinel structure. The peak corresponds to NC retains its position in MNCC indicate the successful coating of nanocellulose on the surface of Fe_3O_4.

The percentage crystallinity of cellulose and NC were compared using the equation (Das et al., 2010):

$$\text{Crystallinity}(\%) = \frac{(I_c - I_a)}{I_c} \times 100 \quad (5)$$

where I_c and I_a are the intensity of the crystalline and amorphous peaks, respectively. The percentage crystallinity was found to be 67.05% for cellulose and 81.74% for NC. The high percentage crystallinity of NC as compared to cellulose was reported by many authors (Das et al., 2010; Rosa et al., 2010).

The crystallite size of NC and MNCC was calculated using Debye–Scherrer's formula (Scherrer, 1918),

$$D = \frac{0.89\lambda}{\beta \cos\theta} \quad (6)$$

where λ is the wavelength of X-rays (1.5406 Å), β is the full width at half-maximum of the XRD peaks and θ is the diffraction angle. The crystallite size of NC and MNCC thus calculated to be 25.0 and 23.8 nm, respectively. This small grain size will increase the surface area and grafting efficiency of the material.

The small shift in the characteristic peak and decrease in the crystallinity of P(MAA-co-VSA)-g-MNCC indicate the successful grafting of P(MAA-co-VSA) onto MNCC. The increased amorphous nature of the adsorbent may improve the hydrophilicity and adsorption capacity. On going through the XRD patterns of Hb-P(MAA-co-VSA)-g-MNCC, we can see that characteristic peaks of P(MAA-co-VSA)-g-MNCC remain intact after the loading of Hb, which is attributed to the fact that the adsorbent is stable in whole of the reaction. Due to the loading of Hb onto P(MAA-co-VSA)-g-MNCC, the crystalline nature of the adsorbent is completely changed.

Dynamic light scattering (DLS) studies (Fig. 3) were carried out to measure the particle size of NC which shows two peaks with average particle size of 80.3 and 358.2 nm. This information clearly indicates that the cellulose nanocrystals which were dispersed by water have the same average diameter (D) of 80.3 and length (L) of 358.2 nm. The dimensions of the cellulose nanocrystals closely match previously reported work of several authors (Bo Bondeson, Mathew, & Oksman, 2006; Filson, Dawson-Andoh, & Schwegler-Berry, 2009). The polydispersity index (PDI) of NC was determined to be 0.522. PDI measurement indicates the width of the particle size distribution and shows the value zero for a highly monodispersed sample and 1 or more for a highly poly-dispersed sample.

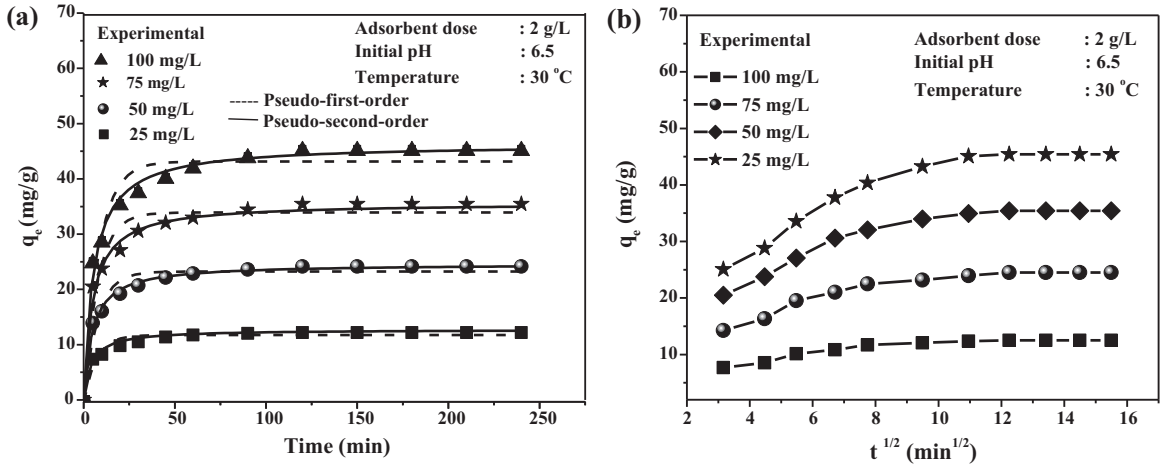

Fig. 4. Adsorption kinetics of Hb adsorption onto P(MAA-co-VSA)-g-MNCC: (a) pseudo-first- and pseudo-second-order kinetic models and (b) intra-particle diffusion model.

The relatively good PDI value obtained for the NC dispersions indicates a high degree of monodispersity of these samples.

3.3. Swelling capability of P(MAA-co-VSA)-g-MNCC

Fig. S2 shows a typical time dependency on swelling of P(MAA-co-VSA)-g-MNCC at different temperatures. It was observed that the swelling ratio of the adsorbent increases with time and levels off to maximum within 2 h. When the temperature was increased from 10 to 40 °C, the swelling ratio was also found to be increased. The reason may be predicted as follows. At low temperatures, polymer chains in solution are hydrated and simply entangled with one another. As temperature increases, macromolecules gradually lose their water of hydration, until polymer–polymer hydrophobic associations take place, thus forming the hydrogel network (Sannino, Demitri, & Madaghiele, 2009).

Supplementary data related to this article found, in the online version, at http://dx.doi.org/10.1016/j.carbpol.2012.11.104.

Swelling ratio of the P(MAA-co-VSA)-g-MNCC increased with increase in pH value, and attained maximum beyond pH 6.0 (inset of Fig. S2). The pK_a of the PMAA is around 4.5 and that of PVSA is around 2.5. When pH is less than pK_a, the H^+ ion strength will be high, which will effectively suppress the ionization of –COOH and $-SO_3H$ groups. So, at acidic pH, the gel is neutral and flexibility of the polymeric chain is rather low. With the increase at pH from 2.0 to 9.0, the ionization of both –COOH and $-SO_3H$ enhanced gradually. As the ionic swelling pressure increases, the composite tends to expand and thereby maximizes the repulsion between the ionized groups, swelling ratio also increases. Increase in the anion density in the P(MAA-co-VSA)-g-MNCC, results in high swelling capacity. A similar observation was reported earlier for the superabsorbent polymer of carboxymethyl chitosan grafted with sodium acrylate and 1-vinyl-2-pyrrolidone (Yu, Yun-fei, Hui-man, & Jieng, 2009)..

3.4. Effect of pH on Hb adsorption

Percentage of adsorption was found to be increased with increasing pH value, reaches a maximum at 6.5 and then decreases (Fig. S3). The isoelectric point (pI) of Hb is about 6.8. At pH values lower than pI, the surface of Hb has positive charge, and above that it has a negative charge. The pH_{zpc} of the adsorbent is in 3.6 and therefore, maximum adsorption at pH 6.5 is due to the electrostatic interaction between the negatively charged adsorbent and positively charged Hb molecule. The maximum recovery of Hb at pH 6.5 was found to be 99.7 and 97.9% at an initial concentration of 25 and 50 mg/L, respectively. The decrease of adsorption capacity may be caused by the increase in conformational size of the protein molecules and the lateral electrostatic repulsions between adjacent adsorbed Hb molecules when deviating from isoelectric point. Thus, these results helped us to select pH 6.5 as the optimum pH for further studies.

Supplementary data related to this article found, in the online version, at http://dx.doi.org/10.1016/j.carbpol.2012.11.104.

3.5. Adsorption kinetics

The effect of contact time on the adsorption of Hb onto P(MAA-co-VSA)-g-MNCC was studied at different concentrations (25–100 mg/L) and the results are shown in Fig. 4. The rapid uptake of Hb was observed at the initial state which may be due to the greater number of reaction sites available for the adsorption of Hb and attained equilibrium at 120 min. With the increase of initial concentration of Hb from 25 to 100 mg/L, the adsorption capacity increases from 12.46 to 45.40 mg/g, indicating that the adsorption of Hb onto P(MAA-co-VSA)-g-MNCC depends on the initial concentration. After 2 h, rise in adsorption capacity was negligible and hence, equilibrium adsorption time for Hb onto P(MAA-co-VSA)-g-MNCC was fixed at 2 h for all the concentrations.

Adsorption process dependent on and is controlled by different kind of mechanisms. In order to clarify the adsorption process, adsorption models such as pseudo-first-order kinetic model, pseudo-second-order kinetic model and intra-particle diffusion model were applied to evaluate the experimental data, as given below:

$$\text{Pseudo-first order} : q_t = q_e(1 - e^{-k_1 t}) \quad (7)$$

$$\text{Pseudo-second order} : q_t = \frac{k_2 q_e^2 t}{1 + t k_2 q_e} \quad (8)$$

$$\text{Intra-particle diffusion} : q_t = k_d t^{1/2} \quad (9)$$

where q_e and q_t (mg/g) are the amount of Hb adsorbed on P(MAA-co-VSA)-g-MNCC at equilibrium and time t (min) respectively. k_1 (min^{-1}) is the rate constant for the pseudo-first-order adsorption process. k_2 (g/mg min) is the rate constant for the pseudo-second order kinetics. K_d (mg/g $min^{1/2}$) is the intra-particle diffusion rate constant. The initial adsorption rate h_0 (mg/g min) from pseudo-second-order kinetic model can be written as:

$$h_0 = k_2 q_e^2 \quad (10)$$

Experimental and theoretical calculated q_e values and coefficients related to pseudo-first-order kinetic model and pseudo-second-order kinetic model are given in Table 1. It

Table 1
Kinetic parameters for the adsorption of Hb onto P(MAA-co-VSA)-g-MNCC.

C_0 (mg/L)	q_e,exp (mg/g)	Pseudo-first-order				Pseudo-second-order				
		k_1 (min^{-1})	q_e,cal (mg/g)	R^2	χ^2	K_2 (g/mg/min)	q_e,cal (mg/g)	h_0 (mg/g min)	R^2	χ^2
25	12.500	0.145	12.070	0.956	0.589	0.019	12.736	3.082	0.992	0.101
50	24.488	0.132	23.562	0.957	2.225	0.008	24.961	4.984	0.994	0.311
75	35.439	0.130	33.921	0.949	5.536	0.005	35.998	6.479	0.991	0.960
100	45.401	0.117	43.477	0.952	8.827	0.004	46.308	8.577	0.992	1.409

was observed that the values of k_1 remain almost constant ($\sim 13.0 \times 10^{-2}\ min^{-1}$) whereas the value of k_2 decreased from 1.9×10^{-2} to 0.4×10^{-2} g/mg min as the initial Hb concentration increased from 25 to 100 mg/L. The closeness of theoretical values (q_e,cal) with experimental data (q_e,exp) ensures the applicability of pseudo-second order kinetic model than pseudo-first order and intra-particle diffusion models. Also, the R^2 values closer to unity and very low χ^2 values, confirmed the applicability of pseudo-second-order kinetic model in the present study, which means that chemisorption is the determining step of the adsorption process rather than mass transfer in solution. Earlier workers also reported similar mechanism which followed pseudo-second-order kinetics for the adsorption of proteins (Ho & McKay, 1999). As the initial Hb concentration increases, the initial adsorption rate (h_0) increases while the rate constant of adsorption (k_2) decreases. In intra-particle diffusion model, the plots of q_e vs $t^{1/2}$ present multi-linearity indicating two or more steps influence the adsorption process. The first step (sharper portion) is as an external surface adsorption or faster adsorption step. In the second step (equilibrium stage), an equilibrium was observed due to the extremely low adsorbate concentrations in the solution. Since there is no intermediate stage, the process may not be controlled by intra-particle diffusion or pore diffusion (Yao, Qi, & Wang, 2010). This behavior indicates that adsorption of Hb had occurred only at the surface of the adsorbent.

3.6. Adsorption isotherm

Adsorption isotherm studies were carried out by varying initial Hb concentrations from 25 to 800 mg/L and temperatures from 10 to 40 °C, for a contact time of 2 h and pH of 6.5. The amount adsorbed gets increased with increase in concentration and temperature from 10 to 40 °C. However, a decreased adsorption capacity was observed beyond 40 °C. At higher temperature, the Hb molecules unfold and causes agglomeration so that the hydrophobic part interact with the hydrophilic part of the adsorbent and decrease the adsorption of Hb at temperature above 40 °C.

The adsorption equilibrium isotherm data is valuable in describing the distribution of adsorbate molecules with the liquid and the solid phases when the adsorption process reaches an equilibrium state. The adsorption data interpretations were done by the nonlinear forms of Langmuir, Freundlich, and Sips isotherms:

$$\text{Langmuir}: q_e = \frac{Q^o b C_e}{1 + bC_e} \tag{11}$$

$$\text{Freundlich}: q_e = K_F C e^{1/n} \tag{12}$$

$$\text{Sips}: q_e = \frac{q_s b_s C_e^{1/n_s}}{1 + b_s C_e^{1/n_s}} \tag{13}$$

where q_s, b_s and $1/n_s$ are sips maximum adsorption capacity, equilibrium constant related to adsorption capacity and surface heterogeneity, respectively. For a highly heterogeneous system, the deviation of $1/n_s$ value from unity will be higher (Sips, 1948).

The experimental isotherms and their corresponding fitting results for Hb adsorption onto P(MAA-co-VSA)-g-MNCC are shown in Fig. 5. The values of isotherm constants were calculated using nonlinear regression analysis, and the results are listed in Table 2. The lower value of χ^2 and closer to unity value of R^2 indicate the better fit isotherm model. The Langmuir isotherm equation (Langmuir, 1918) follows Henry's law at low concentrations and is valid for homogeneous surfaces. The increase in the adsorption capacity and intensity of adsorption with increase in temperature indicates that adsorption is more favorable at high temperatures. The Langmuir fit is considered to be evident that adsorption takes place in monolayer, consistent with specific sorption onto functional binding sites. Freundlich isotherm is suitable for heterogeneous surfaces (Freundlich, 1906). The Freundlich model is characterized by $1/n$, the heterogeneity factor and the value of $0.1 < 1/n < 1.0$ shows the favorable adsorption of Hb onto P(MAA-co-VSA)-g-MNCC. But Freundlich model showed the highest error values when comparing with the experimental results. Sips model equation follows Freundlich isotherm at lower solute concentration and follows Langmuir isotherm at higher solute concentration. The applicability of the isotherm models for the present experimental data approximately follows the order: Sips > Langmuir > Freundlich. The application of the Sips isotherm equation implies a multilayer adsorption at lower concentration of Hb and monolayer adsorption at higher concentration onto P(MAA-co-VSA)-g-MNCC.

3.7. Adsorption thermodynamics

It was found that the adsorption capacity values increased as the temperature was increased. Due to the dependence on temperature, Langmuir constants were used to predict the Gibbs free energy change (ΔG^0), enthalpy change (ΔH^0) and entropy change (ΔS^0). These thermodynamic parameters were determined by using the following equation:

$$\Delta G^0 = \Delta H^0 - T\Delta S^0 \tag{14}$$

$$\ln K_L = \frac{\Delta S^0}{R} - \frac{\Delta H^0}{RT} \tag{15}$$

where ΔG° is the free energy change of specific adsorption (J/mol), R is gas constant (J/K mol), T is the absolute temperature (K), K_L (L/g) is an equilibrium constant obtained by multiplying the Langmuir constants Q^0 and b, ΔS^0 (J/mol K) and ΔH^0 (J/mol) are the standard entropy and enthalpy changes of adsorption, respectively. The plot of $\ln K_L$ versus $1/T$ yields a straight line (figure not shown) from which the values of ΔH^0 and ΔS^0 were calculated from the slope and intercept, respectively. The calculated values of the thermodynamic parameters are given in Table S2. The ΔH^0 value found for the adsorption of Hb was positive due to the endothermic nature of the adsorption process. A negative value of ΔG^0 indicates the spontaneous nature of the reaction, while the positive value for ΔS^0 reflects an increase in the randomness at the solid/solution interface during the adsorption process (Ngah & Hanafiah, 2008). A more negative value of ΔG^0 at higher temperatures were observed in this study, imply greater driving force for adsorption at high temperature (Crini & Badot, 2008).

Supplementary data related to this article found, in the online version, at http://dx.doi.org/10.1016/j.carbpol.2012.11.104.

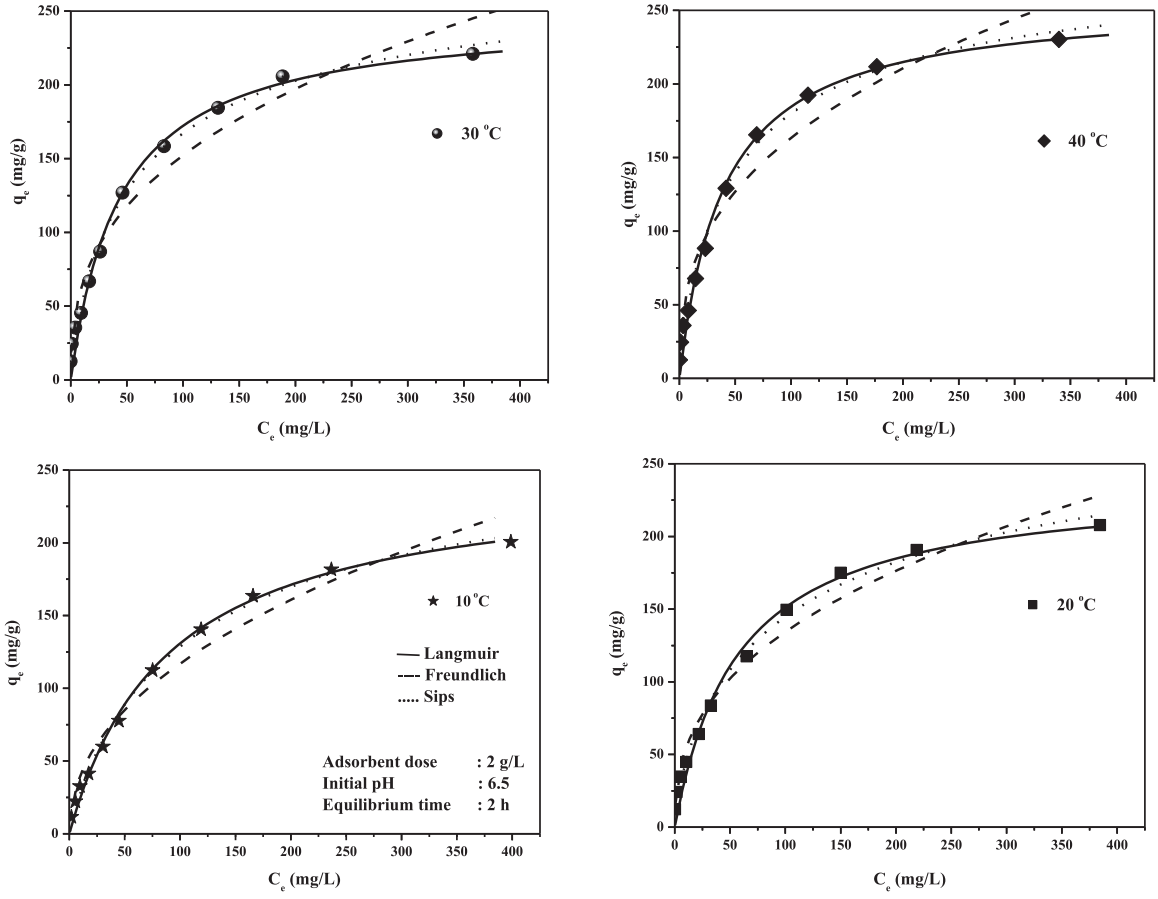

Fig. 5. Isotherm plot for the adsorption of Hb onto P(MAA-co-VSA)-g-MNCC at different temperatures.

3.8. Effect of ionic strength

The effect of ionic strength on the adsorption of Hb onto P(MAA-co-VSA)-g-MNCC was studied by varying the concentrations of NaCl (inorganic salt) and urea (organic salt) and the results are shown in Fig. S4. It is clear from figure that as the ionic strength of NaCl increases from 0.02 to 0.1 M, the extent of adsorption increases from 92.4 to 100%. The reason can be explained as follows. In the presence of NaCl, charged sorbent surfaces and protein macro ions are surrounded by the counter ions (Na^+ and Cl^-). In such systems, adsorption of protein molecules to the charged solid will involve a redistribution of charge in the interfacial region, which in turn affects the adsorption. After binding of the added ions to the active sites on the Hb molecules, repulsion between the Hb and the P(MAA-co-VSA)-g-MNCC surface will be screened. It obviously results in a favorable contact between the Hb and –COOH and $–SO_3H$ groups of the adsorbent. Due to a decrease in the electrostatic repulsion between the protein molecules and P(MAA-co-VSA)-g-MNCC surfaces, the diffusion of Hb molecules will become relatively faster and their attachment to the surface also become easier (Bajpal & Sachdeva, 2002).

Supplementary data related to this article found, in the online version, at http://dx.doi.org/10.1016/j.carbpol.2012.11.104.

However, on increasing the concentration of urea solution from 0.02 to 0.1 M, a decrease in adsorption capacity from 90.3 to 84.3% was observed. This opposite trend may be due to the denaturation of proteins by weakening the hydrogen bonds on interaction with urea, which limits the binding capacity of Hb molecules onto P(MAA-co-VSA)-g-MNCC. In the native state, the heme groups are deeply buried in the hydrophobic pockets of Hb with a five-coordinate high-spin complex (Mueser, Rogers, & Arnone, 2000). In the presence of a denaturant, the fifth coordinative bond between the heme groups and the residue of the polypeptides (His-F8) is broken, and as a result, the heme groups initially buried deeply in the hydrophobic pockets dissociate from the polypeptide chains and the unfolding of Hb takes place (Li et al., 2009). UV–visible spectra (Fig. S5) also confirmed this fact by showing a decrease in intensity of Hb band at 406 nm, which was assigned to the heme monomer coordinated to His-F8 (Hargrove & Olson, 1996), with addition of urea. Also, it is a well-known fact that the strength of interaction between a protein and a surface has been increased with increasing hydrophobicity of the surface and

Table 2
Isotherm parameters for the adsorption of Hb onto P(MAA-co-VSA)-g-MNCC at different temperatures.

Temp. (°C)	Langmuir				Freundlich				Sips				
	Q^0 (mg/g)	b (L/mg)	R^2	χ^2	K_F ($mg^{1-1/n}$ $L^{1/n}$/g)	$1/n$	R^2	χ^2	Q_s (mg/g)	K_s (L/mg)	$1/n_s$	R^2	χ^2
10	237.60	0.011	0.995	25.36	14.06	0.459	0.996	153.35	271.29	0.015	0.888	0.996	22.20
20	247.09	0.017	0.984	87.54	21.91	0.393	0.974	144.51	305.40	0.033	0.715	0.992	50.10
30	248.19	0.022	0.986	87.68	27.32	0.373	0.963	239.48	284.33	0.036	0.799	0.989	73.67
40	257.09	0.025	0.986	93.50	30.37	0.365	0.958	292.58	287.77	0.038	0.817	0.989	82.74

protein (Green, Davies, Roberts, & Tendler, 1997). But, the presence of a hydrophilic organic solvent with low dielectric constant breaks the structure of the water and reduces the hydrophobic interaction (Kubota, Tatsumoto, & Sano, 1999).

Supplementary data related to this article found, in the online version, at http://dx.doi.org/10.1016/j.carbpol.2012.11.104.

3.9. Selective adsorption of proteins

The selectivity of P(MAA-co-VSA)-g-MNCC in the adsorption of proteins was checked by mixing equal amounts of both BSA and Hb solutions. As we know, Hb and albumin are abundant proteins, easily obtained from blood, and are relatively long lived in humans (lifetime ~120 days for Hb and ~21 days for albumin (Troester, Lindstrom, Kupper, Waidyanatha, & Rappaport, 2000). Also, the separation of these proteins is important because of their similar size (Avramescu, Borneman, & Wessling, 2003). As compared to BSA, Hb is stable due to the inaccessibility of the heme center deeply buried in the hydrophobic large peptide backbone, which resists unfolding at normal conditions. As concerning the biological system, albumin and Hb are found in different physiologic compartments, their particular biochemical environments can affect the stability of proteins. Within the red cell, high levels of glutathione (>2 mM) is present, and the sulfhydryl groups from glutathione and proteins can form mixed disulfide bonds that tend to stabilize Hb and protect reactive amino acids from covalent modification (Srivastava, 1971). Because albumin is present in plasma with much lower glutathione concentrations (1–10 μM) and is not protected by the erythrocyte membrane, it would be expected to react more efficiently than Hb (Smith, Jones, Guenthner, Lash, & Lauterburg, 1996).

Here, the adsorption studies were carried out with the protein initial concentrations ranging from 25 to 800 mg/L, at pH 6.5. The adsorption capacities of BSA and Hb on P(MAA-co-VSA)-g-MNCC were determined spectrophotometrically concerning the absorbances measured at 406 nm (for Hb) and 280 nm (for BSA). The adsorption capacities of the proteins on the adsorbent were calculated using the equations:

$$C_A = \frac{K_{B_2} d_1 - K_{B_1} d_2}{K_{A_1} K_{B_2} - K_{A_2} K_{B_1}} \quad (16)$$

$$C_B = \frac{K_{A_1} d_2 - K_{A_2} d_1}{K_{A_1} K_{B_2} - K_{A_2} K_{B_1}} \quad (17)$$

where C represents concentration of proteins adsorbed, A and B represents components in a binary solute system, K_{A_1}, K_{A_2}, K_{B_1} and K_{B_2} are calibration constants for components A and B at λ_1 and λ_2 respectively, d_1 and d_2 are optical densities at λ_1 and λ_2, respectively.

The distribution coefficient, K_D is defined as:

$$K_D = \frac{C_p}{C_s} \quad (18)$$

where C_p (mg/g) is the concentration of protein on P(MAA-co-VSA)-g-MNCC and C_s (mg/L) the concentration of protein in the solution.

The K_D values obtained for Hb and BSA are listed in Table S3. The higher K_D of Hb at pH 6.5 may be due to the conformational stability and high electrostatic attraction as compared to BSA (Zhang, Bai & Tong, 2006). Since BSA lacks competitive power with respect to Hb due to electrostatic repulsion, Hb adsorption is not affected by other component (Avramescu, Borneman, & Wessling, 2003). Thus the results show that P(MAA-co-VSA)-g-MNCC can be utilized for the selective separation of Hb from a mixture of proteins.

Supplementary data related to this article found, in the online version, at http://dx.doi.org/10.1016/j.carbpol.2012.11.104.

3.10. Desorption and regeneration studies

Desorption is an important process in adsorption studies because it enhances the economical value of the adsorption process. Desorption experiments were carried out using 0.01 M KOH, Na_2CO_3, CH_3COOH, Na_2SO_4 and $H_2C_2O_4$ and the percentage of desorption was found to be 99.1, 35.3, 9.0, 21.8 and 12.5%, respectively. Among these, 0.01 M KOH was proved to be the most suitable desorbing reagent. Therefore, adsorption–desorption experiments were conducted with 0.01 M KOH for five cycles and the results are plotted in Fig. S6. During five cycles, the adsorption capacity of P(MAA-co-VSA)-g-MNCC declined from 99.8 to 95.4% and the recovery of Hb molecules in 0.01 M KOH decreased from 99.1% to 93.6%. The loss of adsorbent during five adsorption–desorption cycles was minimal, and this behavior of the P(MAA-co-VSA)-g-MNCC is highly beneficial for the design of a batch reactor. Adsorbent–desorption operations illustrating stabilized performance of the adsorbent in repeated cycles.

Supplementary data related to this article found, in the online version, at http://dx.doi.org/10.1016/j.carbpol.2012.11.104.

4. Conclusions

A novel adsorbent, poly(methacrylic acid-co-vinyl sulfonic acid)-grafted magnetite nanocellulose composite (P(MAA-co-VSA)-g-MNCC) was prepared, by graft copolymerization technique, and well-characterized. Batch adsorption experiments were conducted to find out the efficiency of the adsorbent to recover Hb from aqueous solutions. The effects of adsorbent dose, pH, contact time, initial protein concentration and temperature, on the adsorption of Hb onto P(MAA-co-VSA)-g-MNCC were investigated. The optimum pH for the adsorption of Hb on P(MAA-co-VSA)-g-MNCC was found to be 6.5. Electrostatic interaction had played the determining role in the adsorption of Hb onto P(MAA-co-VSA)-g-MNCC. Hb adsorption on P(MAA-co-VSA)-g-FMNC follows a pseudo-second-order kinetic model, which indicates that adsorption involves chemical interaction. The adsorption isotherm results were well-fitted into Sips and Langmuir isotherm models, which confirm monolayer coverage process at higher concentrations. Higher temperature favored adsorption, indicating that process was endothermic in nature. Satisfactory results were obtained from the attempts for the selective separation of Hb from mixture of proteins. Hb adsorbed onto P(MAA-co-VSA)-g-MNCC could be recovered effectively by treating with 0.01 M KOH solution. The present investigation shows that P(MAA-co-VSA)-g-MNCC can be used as an effective adsorbent for the selective recovery of Hb molecules.

Acknowledgements

The authors thank Department of Chemistry, University of Kerala for providing laboratory facilities. One of our authors Miss. S. R. Rejeena gratefully acknowledges the financial support from the University Grants Commission (New Delhi) granted Major Research Project (MRP F. No. 37-425/2009 (SR)).

References

Abdel, A. M., Zeinab, H., El-Wahab, A., Ibrahim, A. A., & Al-Shemy, M. T. (2010). Characterization of microcrystalline cellulose prepared from lignocellulosic materials. *Bioresource Technology*, *101*, 4446–4455.

Alemdar, A., & Sain, M. (2008). Isolation and characterization of nanofibres from agricultural residues – Wheat straw and soy hulls. *Bioresource Technology*, *99*, 1664–1671.

Anirudhan, T. S., & Senan, P. (2011). Adsorption potential of sulfonated poly(glycidylmethacrylate)-grafted cellulose for separation of lysozyme from aqueous phase: Mass transfer analysis, kinetic and equilibrium profiles. *Colloids and Surfaces A: Physiochemical and Engineering Aspects*, *377*, 156–166.

Anirudhan, T. S., Tharun, A. R., & Rejeena, S. R. (2011). Investigation on poly(methacrylic acid)-grafted cellulose/bentonite superabsorbent composite: Synthesis, characterization, and adsorption characteristics of bovine serum albumin. *Industrial and Engineering Chemistry Research*, *50*, 1866–1874.

Avramescu, M-E., Borneman, Z., & Wessling, M. (2003). Mixed-matrix membrane adsorbers for protein separation. *Journal of Chromatography A*, *1006*, 171–183.

Bajpal., A. K., & Sachdeva, R. (2002). Study on the adsorption of hemoglobin onto bentonite clay surfaces. *Journal of Applied polymer Science*, *85*, 1607–1618.

Bao, Y., Ma, J., & Li, N. (2011). Synthesis and swelling behaviors of sodium carboxymethyl cellulose-g-poly(AA-co-AM-co-AMPS)/MMT superabsorbent hydrogel. *Carbohydrate Polymers*, *84*, 76–82.

Bayramoglu, G., Yilmaz, M., Senel, A. U., & Arica, M. Y. (2008). Preparation of nanofibrous polymer grafted magnetic poly(GMA-MMA)-g-MAA beads for immobilization of trypsin via adsorption. *Biochemical Engineering Journal*, *40*, 262–274.

Bo Bondeson, D., Mathew, A., & Oksman, K. (2006). Optimization of the isolation of nanocrystals from microcrystalline cellulose by acid hydrolysis. *Cellulose*, *13*, 171–180.

Capadona, J. R., Shanmuganathan, K., Trittsuchuh, S., Seidel, S., Rowan, S. J., & Weder, C. (2009). Polymer nanocomposites with nanowhiskers isolated from microcrystalline cellulose. *Biomacromolecules*, *10*, 712–716.

Crini, G., & Badot, P. -M. (2008). Application of chitosan, a natural aminopolysaccharide, for dye removal from aqueous solutions by adsorption processes using batch studies: A review of recent literature. *Progress in Polymer Science*, *33*, 399–447.

Cruz, J. C., Pfromm, P. H., Tomich, J. M., & Rezac, M. E. (2010). Conformational changes and catalytic competency of hydrolases adsorbing on fumed silica nanoparticles: II. Secondary structure. *Colloids and Surfaces B: Biointerfaces*, *81*, 1–10.

Das, K., Roy, D., Banerjee, C., Bandyopadhyay, N. R., Sahoo, S., Mohanty, A. K., et al. (2010). Physicochemical and thermal properties of jute-nanofiber-reinforced biocopolyester composites. *Industrial and Engineering Chemistry Research*, *49*, 2775–2782.

Dias, A. M. G. C., Hussain, A., Marcos, A. S., & Roque, A. C. A. (2011). A biotechnological perspective on the application of ironoxide magnetic colloids modified with polysaccharides. *Biotechnology Advances*, *29*, 142–155.

El-Safty, S., Shahat, A., & Nguyen, H. (2011). Nano model memebrane filters for the well controlled separation of biomolecules. *Colloids and Surfaces A: Physiochemical and Engineering Aspects*, *377*, 44–53.

Fargues, C., Bailly, M., & Grevillot, G. (1998). Adsorption of BSA and hemoglobin on hydroxyapatite support: Equilibria and multicomponent dynamic adsorption. *Adsorption*, *4*, 5–16.

Filson, P. B., Dawson-Andoh, B. E., & Schwegler-Berry, D. (2009). Enzymatic-mediated production of nanocrystals from recycled pulp. *Green Chemistry*, *11*, 1808–1814.

Freundlich, H. M. F. (1906). Over the adsorption in solution,. *Journal of Physical Chemistry*, *57*, 385–470.

Green, R. J., Davies, J., Roberts, C. J., & Tendler, S. J. B. (1997). Surface plasmon resonance for real time in situ analysis of protein adsorption to polymer surfaces. *Biomaterials*, *18*, 405–413.

Hargrove, M. S., & Olson, J. S. (1996). The stability of holomyoglobin is determined by heme affinity. *Biochemistry*, *35*, 11310–11318.

Haynes, C. A., & Norde, W. (1994). Globular proteins at solid/liquid interfaces. *Colloids and Surfaces B: Biointerfaces*, *2*, 517–566.

Ho, Y. S., & McKay, G. (1999). Pseudo-second-order model for sorption process. *Process Biochemistry*, *34*, 451–469.

Ishiguro, R., Yokoyama, Y., Maeda, H., Shimamura, A., Kameyama, K., & Hiramatsu, K. (2005). Modes of conformational changes of proteins adsorbed on a planar hydrophobic polymer surface reflecting their adsorption behaviors. *Journal of Colloid and Interface Science*, *290*, 91–101.

Joon, T. O., & Kim, J. H. (2000). Preparation and properties of immobilized amyloglucosidase on nonporous PS/PNaSS microspheres. *Enzyme and Microbial Technology*, *27*, 356–361.

Kubota, N., Tatsumoto, N., & Sano, T. (1999). Recovery of serum proteins using cellulosic affinity membranes modified with tannic acid. *Carbohydrate Polymers*, *40*, 107–113.

Kundakci, S., Uzum, O. B., & Karadag, E. (2008). Swelling and dye sorption studies of acrylamide/2-acrylamido-2-methyl-1-propanesulfinic acid/bentonite highly swollen composite hydrogels. *Reactive and Functional Polymers*, *68*, 458–473.

Langmuir, I. (1918). The adsorption of gases on plane surfaces of glass, mica and platinum. *Journal of the American Chemical Society*, *40*, 1361–1403.

Li, X., Zheng, W., Zhang, L., Yu, P., Lin, Y., Su, L., et al. (2009). Effective electrochemical method for investigation of hemoglobin unfolding based on the redox property of heme groups at glassy carbon electrodes. *Analytical Chemistry*, *81*, 8557–8563.

Mueser, T. C., Rogers, P. H., & Arnone, A. (2000). Interface sliding as illustrated by the multiple quaternary structures of liganded hemoglobin. *Biochemistry*, *39*, 15353–15364.

Mulinari, D. R., & Da Silva, M. L. P. (2008). Adsorption of sulphate ions by modification of sugarcane bagasse cellulose. *Carbohydrate Polymers*, *74*, 617–620.

Ngah, W. S. W., & Hanafiah, M. A. K. M. (2008). Adsorption of copper on rubber (*Hevea brasiliensis*) leaf powder: Kinetics equilibrium and thermodynamic studies. *Biochemical Engineering Journal*, *39*, 521–530.

Nishino, T., Matsuda, I., & Hirao, K. (2004). All cellulose composite. *Macromolecules*, *37*, 7683–7687.

Nyquist, R. A., & Kagel, R. O. (1971). *Infrared spectra of inorganic compounds (3800–45 cm^{-1})*. New York: Academic Press.

Pal, K., Banthia, A. K., & Majumdar, D. R. (2009). Polymeric hydeogels: Characterization and biomedical applications – A mini review. *Designed Monomers and Polymers*, *12*, 197–220.

Peng, Z. G., Hidajat, K., & Uddin, M. S. (2004). Adsorption and desorption of lysozyme on nanosized magnetic particles and conformational changes. *Colloids and Surfaces B: Biointerfaces*, *35*, 169–174.

Rosa, M. F., Medeiros, E. S., Malmonge, J. A., Gregorski, K. S., Wood, D. F., Mattoso, L. H. C., et al. (2010). Cellulose nanowhiskers from coconut husk fibers: Effect of preparation conditions on their thermal and morphological behavior. *Carbohydrate Polymers*, *81*, 83–92.

Sannino, A., Demitri, C., & Madaghiele, M. (2009). Biodegradable cellulose-based hydrogels: Design and applications. *Materials*, *2*, 353–373.

Scherrer, P. (1918). Bestimmung der Grösse und der inneren Struktur von Kolloidteilchen mittels Röntgenstrahlen. *Nachrichten von der Gesellschaft der Wissenschaften zu Göttingen*, *26*, 98–100.

Schwarz, J. A., Driscoll, C. T., & Bhanot, A. K. (1984). The zero point charge of silica–alumina oxide suspension. *Journal of Colloid and Interface Science*, *97*, 55–61.

Shukoor, M. I., Natalio, F., Tahir, M. N., Ksenofontov, V., Therese, H. A., Theato, P., et al. (2007). Superparamagnetic-Fe_2O_3 nanoparticles with tailored functionality for protein separation. *Chemical Communication*, 4677–4679.

Sips, R. (1948). On the structure of a catalyst surface. *Journal of Chemical Physics*, *16*, 490–495.

Smith, C. V., Jones, D. P., Guenthner, T. M., Lash, L. H., & Lauterburg, B. H. (1996). Compartmentation of glutathione: Implications for the study of toxicity and disease. *Toxicology and Applied Pharmacology*, *140*, 1–12.

Srivastava, S. K. (1971). Metabolism of red cell glutathione. *Experimental Eye Research*, *11*, 294–305.

Troester, M. A., Lindstrom, A. B., Kupper, L. L., Waidyanatha, S., & Rappaport, S. M. (2000). Stability of hemoglobin and albumin adducts of benzene oxide and 1,4-benzoquinone after administration of benzene to F344 rats. *Toxicological Sciences*, *54*, 88–94.

Yao, Z.-Y., Qi, J.-H., & Wang, L.-H. (2010). Equilibrium, kinetic and thermodynamic studies on the biosorption of Cu(II) onto chestnut shell. *Journal of Hazardous Materials*, *174*, 137–143.

Yokoyama, Y., Ishiguro, R., Maeda, H., Mukaiyama, M., Kameyama, K., & Hiramatsu, K. (2003). Qunatitaive analysis of protein adsorption on a planar surface by Fourier transform infrared spectroscopy: Lysozyme adsorbed on hydrophobic silicon-containing polymer. *Journal of Colloid and Interface Science*, *268*, 23–32.

Yu, C., Yun-fei, L., Hui-man, T., & Jieng, J. (2009). Synthesis and characterization of a novel superadsorbent polymer of N,O-carboxy-methyl chitosan graft copolymerized with vinyl monomers. *Carbohydrate Polymers*, *75*, 287–292.

Zhang, X., Bai, R., & Tong, T. W. (2006). Selective adsorption behaviors of proteins on polypyrrole-based adsorbents. *Separation and Purification Technology*, *52*, 161–169.